Microsyst Technol (2014) 20:427–436
DOI 10.1007/s00542-013-1972-z

TECHNICAL PAPER

Rapid prototyping of magnetic valve based on nanocomposite Co/PDMS membrane

Akanksha Singh · Laurent Hirsinger · Patrick Delobelle · Chantal Khan-Malek

Received: 11 April 2013 / Accepted: 7 November 2013 / Published online: 29 November 2013

Abstract In this study, a new type of active membrane based on magnetic elastomer composite is manufactured, characterized and integrated into a simple valve. The simple and low-cost fabrication process combined with large displacement capability of the membrane is favorable for use in disposable fluidic devices. Passivated ferromagnetic cobalt nanoparticles (~37 nm) synthesized by the chemical route were embedded in polydimethylsiloxane (PDMS) to fabricate nano-composite flexible membranes. Magneto-mechanical and mechanical properties of the PDMS composite elastomeric membrane loaded with various concentrations of cobalt (Co) nanoparticles (between 15 and 75 % by weight) were studied. Dynamic mechanical analysis (DMA) measurements of the nanocomposite membranes were conducted as a function of the applied frequency (between 0.1 and 56 Hz). With higher concentration (50-wt%) of Co nanoparticles in PDMS, the elastic modulus was increased by 3–4 times as compared with that of membranes with lower concentrations of nanoparticles. Shore hardness was maximum for the nano-composite membrane loaded with 50-wt% of Co nanoparticles. A fluidic actuator with 400 μm thick PDMS membrane of 18 mm free diameter loaded with 50-wt% Co nanoparticles was manufactured and tested under external magnetic field. In the region where the magnetic field gradient is highest, high deflection of the membrane could be obtained (0.68 mm for 1 Tesla). However some hysteresis of the membrane deflection could be observed, even at very low frequency. Loading of PDMS with Co nanoparticles allowed a wider range of control of the wetting properties of PDMS surfaces under oxygen plasma treatment, from hydrophobic to hydrophilic to super-hydrophilic. Tunability in hydrophilicity could be achieved by varying the process parameters as verified by contact angles and Fourier transforms infrared (FTIR) spectra before and after plasma treatment. Under certain conditions, 50 % Cobalt-PDMS membrane surfaces exhibited a super-hydrophilic behavior (contact angle ~5°).

A. Singh · L. Hirsinger · P. Delobelle · C. Khan-Malek
FEMTO-ST Institute, UMR CNRS 6174/Département MN2S,
32 Avenue de l'Observatoire, 25044 Besançon cedex, France

Present Address:
A. Singh (✉)
Department of Materials Science & Engineering and Micronova,
Aalto University, P.O. Box 13500, FI-00076 Aalto, Finland
e-mail: ebox.akanksha@gmail.com

1 Introduction

Magnetic-based actuator can generate large force and large displacement compared with electrostatic and piezoelectric ones. Elastomeric polymer such as polydimethylsiloxane (PDMS) exhibit the low elastic modulus needed for providing the flexibility of membranes for magnetic actuation to be effective at small scale (Bohm et al. 2001; Khoo and Liu 2001; Yufeng et al. 2006; Yamahata et al. 2005; Oh and Ahn 2006; Lee and Lee 2007; Yin et al. 2007; Gaspar et al. 2008). However, there is an increased need for low cost, fully integrated and remotely controllable actuation technologies at the micro and nanoscale, which can be achieved using a membrane made of magnetically responsive materials. Use of magnetic membranes in active devices is also convenient as they can be actuated externally without the need of any direct connections or wiring, allowing for contact-less operation, which not only eases operation but can also

bring down the cost of devices. A number of groups have developed fluidic actuators such as micro-valves and micro-pumps based on magnetic silicone elastomeric membranes, based mostly on loading the silicone elastomeric with magnetic powder (Jackson et al. 2001), or embedding small magnets embedded in the membrane (Bohm et al. 2001; Khoo and Liu 2001; Yufeng et al. 2006; Yamahata et al. 2005) or glued to it (Bohm et al. 2001) or using embedded coils (Lee and Lee 2007; Yin et al. 2007).

However, there are few reports on magnetic membranes based on nanoparticles (NPs) (Berthier and Ricoul 2004; Fahrni et al. 2009; Pirmoradi et al. 2010). Magnetic membranes showing large and reproducible deflection that can be operated under relatively low magnetic field are desirable for many applications, in particular for microfluidic devices. Berthier and Ricoul have reported membranes using commercial iron particles of ~4 μm size and iron oxide (maghemite γ-Fe_2O_3) particles of 10 nm size dispersed in PDMS (Berthier and Ricoul 2004; Gaspar et al. 2008). The deflections observed in their case were ~200–300 μm with a non-linear response to the magnetic field. Recently magnetic membranes using commercial superparamagnetic iron-oxide nanoparticles (10 nm) have been fabricated by Fahrni (2009) and Pirmoradi (2010). The first group used the nanoparticles with 5-wt% concentration by volume in PDMS and studied the mechanical properties of the fabricated membrane. They showed that the Young's modulus decreased with increasing particle concentration. They also described the magnetic behaviour of the composite polymer. The second group coated these commercial nanoparticles with fatty acid to overcome the agglomeration problem of oxide particles in polymer and made membranes with different diameters from 4 to 7 mm. They achieved ~625 μm deflection under ~0.417 Tesla of magnetic field.

In this work, we report on the manufacture of new nanopolymer composite magnetic membranes based on coated Co nanoparticles embedded with various concentrations in polydimethylsiloxane (PDMS). These membranes have been characterized mechanically and visco-magneto elastically using DMA and durometer hardness test. In addition, one of the key issues is surface wettability of the channel walls in microfluidic devices as most polymers exhibit hydrophobic property and need treatment to become hydrophilic. Therefore, we also studied the surface wettability of these membranes under various plasma conditions and compared it with bare PDMS membrane, using contact angle measurement of water droplet and Fourier Transform spectrometry (FTIR). The membranes were finally integrated as diaphragm in a simple PDMS-based valve and the functionality of the fluidic actuator was tested under varied magnetic field.

2 Experimental section

2.1 Fabrication and characterization of nano-polymer composite magnetic membrane

2.1.1 Magnetic composite membrane

As-synthesized oleic acid-capped Co magnetic nanoparticles of ~37 nm average size and Sylgard 184 PDMS (Dow Corning, MI, USA) were used for the fabrication of magnetic membranes. Detailed description of nanoparticles synthesis and characterization of the nanoparticles are described elsewhere (Singh et al. 2013). In our previous work, the Co nanoparticles were produced in a two-step synthesis different from the one used for oleic acid-stabilized cobalt and iron oxide NPs (Evans et al. 2007; Yang et al. 2004; Yu et al. 2006).

Membranes of 2.5 cm diameter and 3 mm thickness with various weight percentages of nanoparticles (15, 25, 50 and 75 %) with respect to PDMS were prepared in a two-step process. The silicone rubber base was first added to the curing agent in 10:1 ratio by weight and mixed properly. Appropriate quantity of magnetic nanoparticles powder was added to a constant volume of PDMS mixture and again properly mixed and degassed under the primary vacuum for 2–3 h to completely remove any air trapped in the PDMS mixture. The resulting mixture was cast in a Teflon mold and cured at 120 °C for 15 min and cooled down to room temperature. The membrane was carefully demolded. With highly loaded membranes (beyond 50-wt%), the weight of magnetic nanoparticles being higher than that of PDMS solution, it is quite difficult to form a homogenous, smooth membrane and the nanoparticles cluster together. Moreover, the surface of the highly loaded (75-wt%) composite piece is not smooth and there are lots of air bubbles in the cured membrane even after long degassing (4 h compared with 1–1.5 h for lower concentration of nanoparticles).

2.1.2 Optical inspection and surface roughness measurement

All the fabricated membranes were viewed under 3D-optical microscope of Hi-Scope, Compact Micro Vision System (model-KH 2200).

Surface measurements were done using a surface profiler of KLA Tencor (Alpha-Step IQ).

2.1.3 Oxygen plasma treatment of the membranes

Plasma treatment was carried out in inductively coupled plasma (ICP) lab-built plasma system similar in design to the one reported by d'Agostino(1990). The plasma reactor is co-actively coupled to the RF power supply (power

supply system INC, Model ACG-5), which operates at the fixed frequency of 13.56 MHz and has a maximum power output of 555 W. A high power DC supply (from APLAB, 7,341 N) of maximum power output of 3.5 kV was used for sputtering. The flow of oxygen gas was controlled by flow meters having a range of gas flow from 0 to 150 sccm (standard cubic centimeter per minute) and a needle valve connected in series with the flow line. The pressure of the discharge was controlled by the needle valve. The samples were placed on a copper plate. The parameters varied for the experiments of our present study were the chamber pressure, RIE power, and exposure time to oxygen plasma.

Surface wettability of the magnetic NP-embedded membranes and bare PDMS for comparison were studied by measuring the static contact angle using a calibrated water droplet of 5 µl on the various surfaces.

2.1.4 Dynamic mechanical analysis (DMA)

Dynamic mechanical analysis (DMA) is a technique, used to measure the visco-elastic properties, i.e. the stiffness and damping properties of cobalt-PDMS nanocomposite membrane. DMA works by applying a displacement on top of a sample in a cyclic manner (sinusoidal wave with a defined frequency). The transmitted force through the sample is measured at its bottom where the sample is clamped to the mechanism. The strain can be calculated from the applied displacement and the stress from the measured force and the constant section of the sample. The magnitude of the applied stress and the resultant strain are used to calculate the stiffness of the material (Young's modulus).

Testing of magnetic composite slabs was conducted using Bose instrument ELF 3200 (ElectroForce™) and the WinTest DMA software. All the samples used were of the same width (about 8 mm), thickness (about 3 mm) and length (about 18 mm) under the same conditions. DMA tests were carried out on composite PDMS slabs with different concentration of cobalt NPs: 16, 25, 50 and 75 % by weight. Samples made of pristine PDMS have been characterized to give a reference.

2.2 Design and fabrication of valve with magnetic composite nanoparticle-PDMS actuator

A simple flow-through valve has been designed to demonstrate the feasibility of magnetic actuation with the nanoparticles composite membranes. To apply the principle of magnetic actuation in a valve, the overall volume displacement needs to be as large as possible under a given magnetic field and membrane dimensions. The schematic design and side view of the magnetic valve subjected to the magnetic field H and its gradients for the magnetic valve are given in Fig. 1. We can observe that the inner diameter

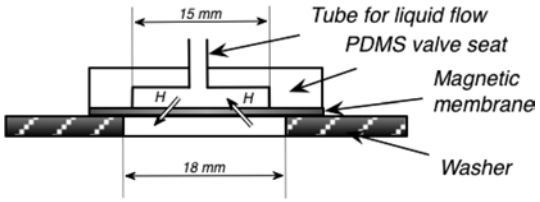

Fig. 1 Schematic diagram and side view of the magnetic valve subjected to the magnetic field *H* and its gradients

of the valve body is of 15 mm and outer diameter is of 35 mm.

The new magnetically driven prototype valve consists of the thin cobalt composite magnetic membrane mounted on top of the pristine PDMS valve body. The mold of the valve body was mechanically milled in aluminum (Fig. 2a). The valve body was manufactured by casting Sylgard 184, PDMS (see description above) (Fig. 2b). The membrane was also cast with a thickness of 400 µm and was made with 50-wt% of Co nanoparticles. Its free diameter, that is to say the membrane diameter that can move freely, corresponds to 18 mm. It is determine by the inner diameter of the washers added on both sides of the valve body as we can see in Fig. 3. These two washers were used to tighten the assembly and make it leak-free. The other side of the valve has been attached to a tube (Fig. 3). Permanent sealing of the nanocomposite Co-PDMS membrane to the PDMS valve body could be achieved using oxygen-plasma. The solution with tightening between two plates was preferred at this stage because it allowed changing membranes if necessary.

2.3 Magnetic test of the valve

Testing of the valve under magnetic field was performed using electromagnets from Brucker. The maximum magnetic field between the poles of the magnet for the actuation of membrane was varied from 0 to 2 Tesla. The magnetic field inside the electromagnet gap was measured with a probe using a Gauss-meter. By applying the magnetic field, the magnetic membrane deflects and fluid flow occurs in the channel.

3 Results and discussion

Figure 4 shows the cross-section of PDMS Co-loaded membranes with the same magnification (50×). The membrane with the highest Co concentration (75-wt%) clearly shows the presence of air-bubbles in the sample thickness. Table 1 lists the roughness data for the various membranes. The roughness increases with higher concentration of nanoparticles.

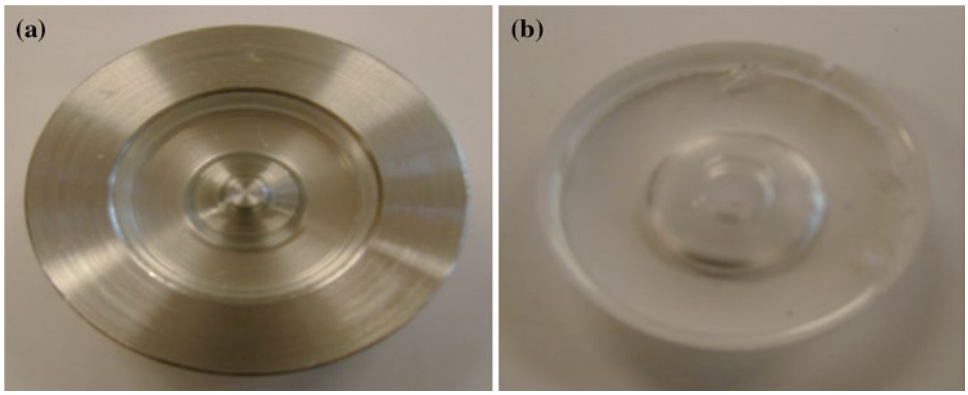

Fig. 2 Optical image of the **a** the mold of the valve body in aluminium and **b** the PDMS replica used for actuator device

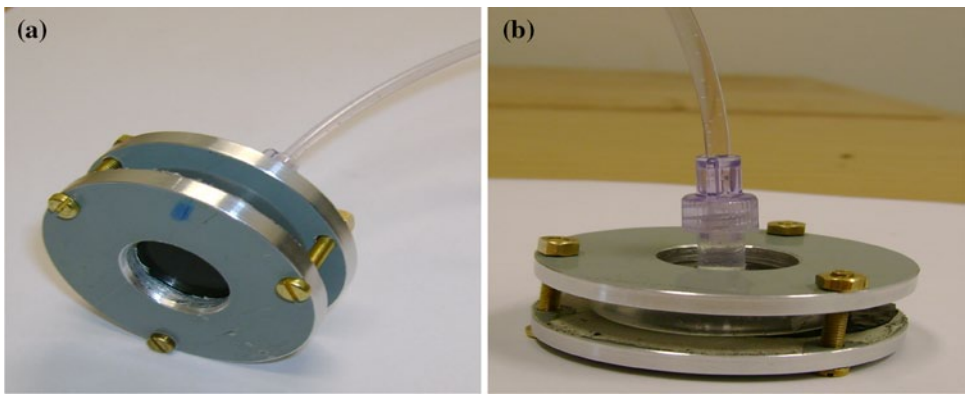

Fig. 3 Actuator device **a** top view and **b** side view

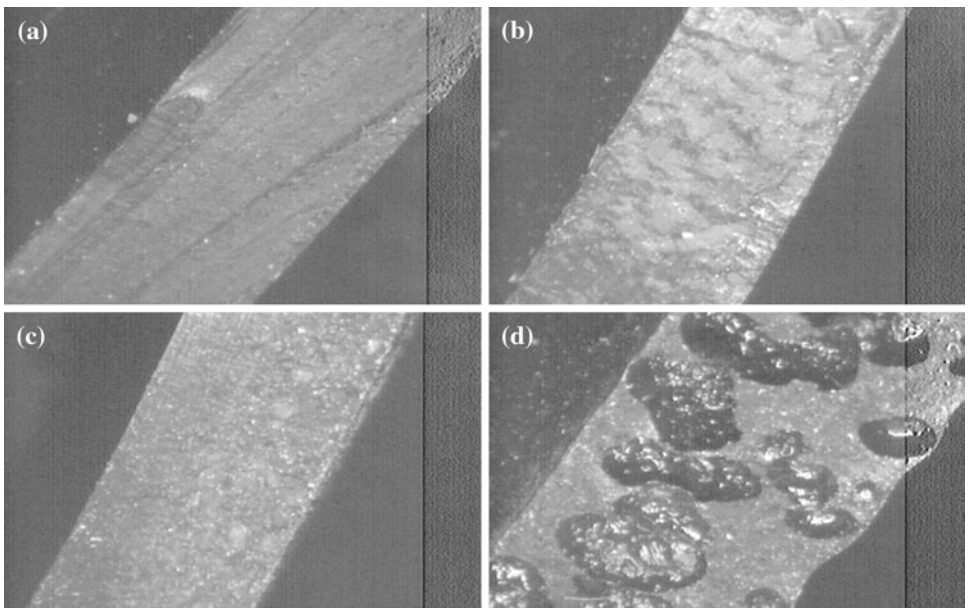

Fig. 4 3-D image (×50) of cross-section of Co nanoparticle embedded PDMS membrane using optical microscope: **a** 15-wt%, **b** 25 wt%, **c** 50-wt% and **d** 75-wt%

The hardness of plastics is most commonly measured with an apparatus known as a Durometer, consequently it is also known as 'Durometer hardness' that may be defined as a material resistance to permanent indentation. Durometer, like many other hardness tests, measures the depth of an indentation in the material created by a given force on a standardized presser foot. This depth is dependent on the hardness of the material, its visco-elastic properties, the shape of the presser foot, and the duration of the test. Table 2 shows the surface hardness (expressed in Shore A

Table 1 Comparison of PDMS membrane roughness from surface profiler (a) 15 wt%, (b) 25 wt%, (c) 50 wt% and (d) 75 wt%

Co-membrane	15 wt%	25 wt%	50 wt%	75 wt%
Ra (arithmetic roughness)	0.040	0.116	0.014	0.17
Rq (root mean square roughness)	0.050	0.144	0.022	0.21
Rt (peak to valley roughness)	0.313	1.4	0.325	2.30

Table 2 Comparison of surface hardness of membranes using durometer pristine PDMS; loaded PDMS with (a) 15 wt%, (b) 25 wt%, (c) 50 wt% and (d) 75 wt%

Membrane	Hardness (Shore A)
Virgin PDMS	54
PDMS-Co-15 wt%	60
PDMS-Co-25 wt%	65
PDMS-Co-50 wt%	72
PDMS-Co-75 wt%	41

scale) of the various PDMS membranes. The surface hardness increases with higher content of Co nanoparticles, except for 75-wt% due to the presence of air bubbles.

Pristine untreated PDMS is hydrophobic in nature and has a contact angle of 120° which is consistent with data from the literature. In the first set of experiments, the wettability of the Co nanoparticle-loaded membranes was studied as a function of RF power (10–50 W) and exposure time (5–30 min) at a constant gas flow rate (10 cc/min). The wettability of the composite PDMS surfaces is found to increase with increasing RF power and exposure time as shown in Fig. 5 for the 50-wt% Co-PDMS membrane.

At a certain optimum value of power and time, the surface becomes super-hydrophilic (contact angle ~5°). As the exposure time to O_2 increases, the carrier molecules become active and the charged particles formed near the electrode move closer to the substrate. So, there is formation of silanol group (–OH) on the surface, making it hydrophilic. A low RF power leads to a reduced kinetic energy of ions incident on the substrate and a lower plasma density. Thus, less active sites form on the sample surface, leading to a reduction in Si–OH groups available for surface bondage. The reverse behavior observed at high RF power suggests an increase in the ion bombardment. It is also observed that the contact angle becomes almost constant when the exposure time to O_2 varies from 15 to 20 min (Fig. 5). But after that there is a sudden fall in the contact angle. The surface becomes super-hydrophilic when the exposure time increases to 30 min. For comparison, bare PDMS membrane is also exposed to oxygen plasma with RF power varying from 10 to 40 W for a fixed

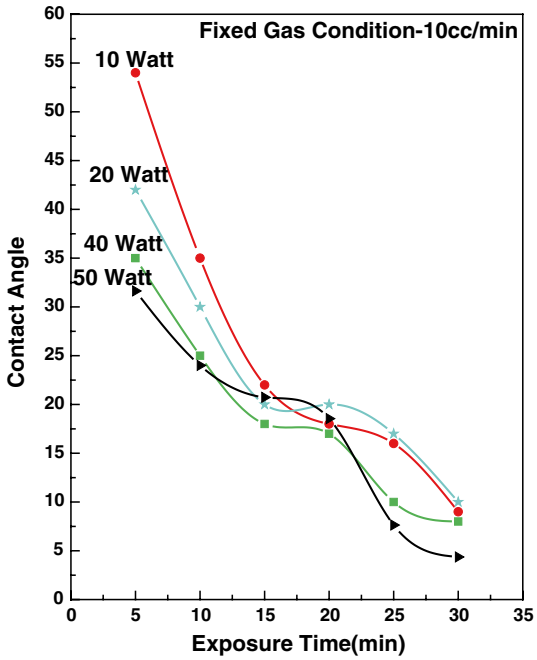

Fig. 5 Contact angle measurement of 50-wt% Co-PDMS membrane at different oxygen plasma exposure times while varying RF power supply

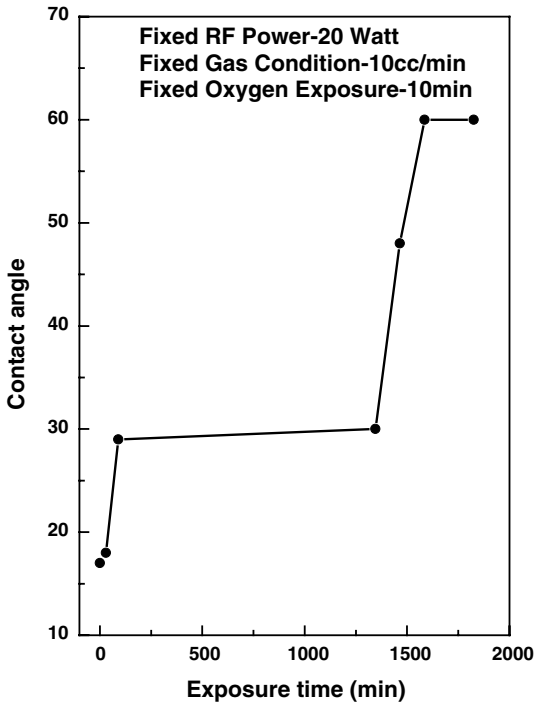

Fig. 6 Contact angle measurement of 50-wt% Co-PDMS membrane at exposure time in atmosphere at constant RF power of 10 W and gas exposure for 10 min

period of time (30 min) while keeping the oxygen flow rate at 10 cc/min and its wettability is found to increase with an increase in RF power (contact angle varying between 120°

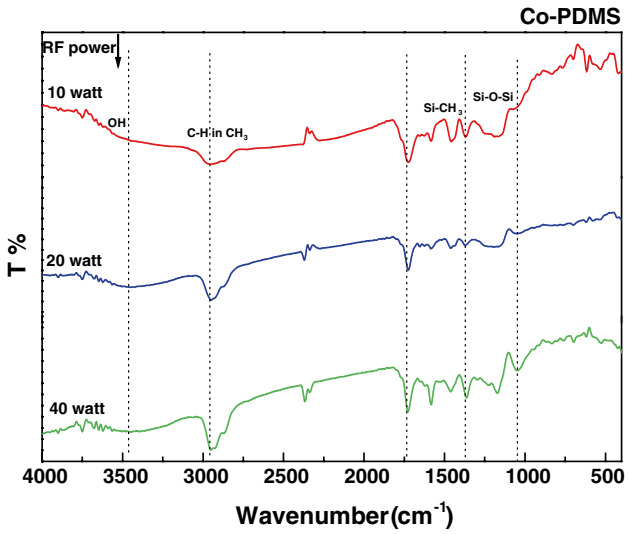

Fig. 7 FTIR plot of 50-wt% Co-PDMS membrane at varying RF power supply after O_2 exposure for 30 min

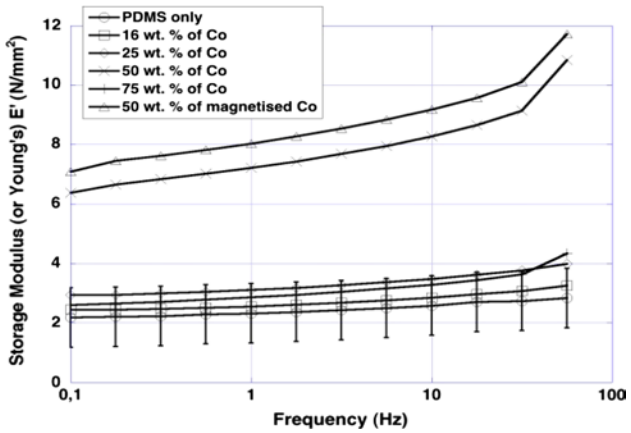

Fig. 8 Dynamical Mechanical Analysis (DMA): elastic (or Young's) modulus versus frequency for PDMS and PDMS loaded with Co nanoparticles at different weight %

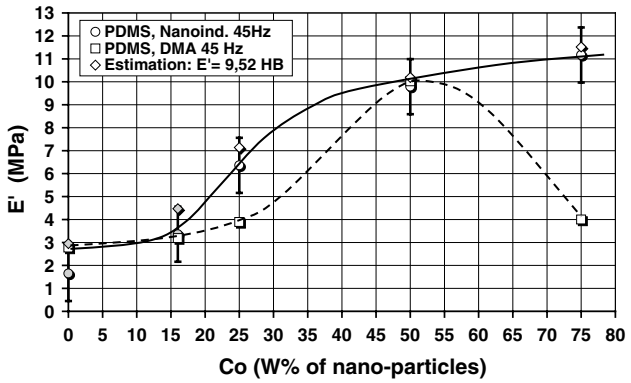

Fig. 9 Evolution of the elastic (or Young's) modulus E' measured by Nano-indentation test and by Dynamical mechanical analysis (DMA) versus the nanoparticles concentration

and 25°), rendering the treated surface hydrophilic. However, this hydrophilic PDMS surface reverses to its initial hydrophobic nature in about a few minutes, as reported in the literature.

In the second set of experiments, the composite 50-wt% Co-PDMS membrane surface was treated with 20 W RF power under 10 cc/min O_2 for 10 min. We observed that with this set of parameters, it remained hydrophilic after exposure in air for more than 1 day (Fig. 6). The contact angle increases from 18° to 60° as a function of exposure time in air but maintains its hydrophilic nature.

Figure 7 shows the FTIR spectra of plasma-treated 50-wt% Co-loaded PDMS membrane and important characteristic peaks are assigned in the spectra. The absorption peaks of C–H in methyl groups (CH_3), Si–CH_3 (side chain of PDMS) and Si–O–Si (main chain) occur at 2,960, 1,270 and 1,020 cm^{-1}, respectively. The spectrum of plasma-treated composite membrane is compared with that of plasma-treated bare PDMS (native bare PDMS being defined as the reference). It is observed that the absorptions due to C=O bonding and that due to O–H in H_2O appear while those due to C–H in CH_3 and that due to Si–CH_3 decrease with the O_2 plasma treatment power. This analysis is consistent with the more hydrophilic behavior of the PDMS loaded with Co nanoparticles.

DMA tests were carried out on composite PDMS slabs with varying concentration of cobalt nanoparticles to study the magneto-mechanical properties of the PDMS/Co nanoparticle composite elastomeric membrane. Samples made of pristine PDMS have been characterized to give a reference. Figure 8 shows DMA measurements of the elastic modulus (or the Young's modulus) as a function of the applied frequency that is varied between 0.1 and 56 Hz. Error bars are used to indicate the storage modulus variation due to the fabrication process fluctuation in pristine PDMS membrane. We can observe the highest storage modulus of 6.5–11 MPa for the 0.1–56 Hz excitation frequencies for cobalt NP composite slab with the concentration of 50-wt% of nanoparticles. This modulus is increased by 3–4 times in comparison with the membranes loaded with a lower concentration of Co nanoparticles. With a concentration beyond 50-wt% of nanoparticles in PDMS, we could not fabricate homogenous membranes. Moreover, the surface of the composite piece is not smooth and includes lots of air bubbles. The presence of air bubbles decreases the real section of the sample and the apparent modulus is reduced as we have seen in Fig. 1 with 75-wt% of Co.

Nano-indentation tests have been carried out to verify this hypothesis and the results, Young's modulus as a function of the Co percentage, is reported in Fig. 9. Indeed, for wt%

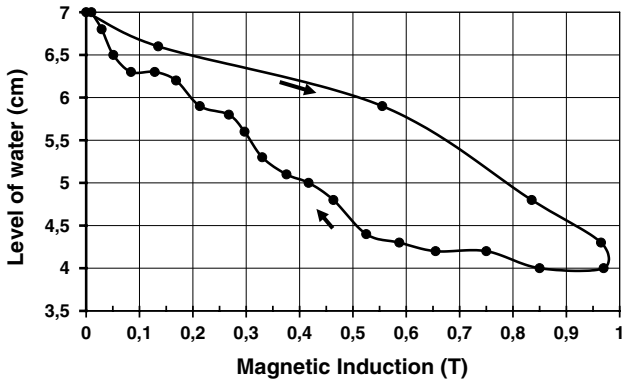

Fig. 10 Hysteresis plot of the fluid level in the fluidic device under magnetic field

(Co) <50 % the values obtained by DMA and nano-indentation procedure are close to each other (specimens without bubble) but for wt% = 75 %, the values greatly diverge. In fact nano-indentation tests are performed at a micro scale (maximal indentation depth of 4 μm) and consequently the bubbles have no effect on the results. On the contrary, DMA tests are performed at a macro scale and the presence of bubbles greatly affects the mean value of the measured Young's modulus. The true Young's modulus of the material is an increasing function of the nanoparticles content.

The fluidic device was placed on one side of the electromagnet with the magnetic membrane facing the electromagnet gap. In this place near the magnetic poles edge, the magnetic field is non-uniform and causes the magnetic membrane to deflect. Under no magnetic field, the default mode for the membrane is the rest mode. When the magnetic field is increased between the electromagnet, the magnetic membrane is actuated and deflects outward leading to a decrease in the water level (Fig. 10). Membrane displacement is caused by the attraction between magnetic nanomaterial (embedded within the PDMS membrane) and the poles of the electromagnet. The experiment started with nearly zero magnetic field (i.e. 0.012 T) between the electromagnet. It can be observe that at this stage, the water level is at 7 cm on the scale (Fig. 10). After that we start the magnetic field inside the magnetic poles up to 1.94 T and at the final stage, the water level decreases down to nearly 4 cm. Testing of our device was done up to 2 T magnetic field, which is sufficient in producing the large displacement of the membrane. The magnetic field in device corresponds to the one measured inside the magnetic poles. To obtain the true value that is applied to the membrane, it needs to divide it by about a factor 2.

Figure 10 shows the hysteresis plot of the data collected by following the liquid level in the device during the increasing and decreasing magnetic field. The maximum deflections were observed when the valve with the tube was set in the horizontal plane to avoid the effect of gravity on water. If the valve and the tube are set vertically with the membrane facing the electromagnet downwards, the fluid mass via the pressure constrained the membrane with a value that can be more important than the magnetic pressure. In this case, the magnetic field is not sufficient to deform the membrane and to push the liquid in the tube. The same thing happens when the membrane is put under tensile strength during the assembly step of the valve. Indeed, a large tensile strength of the membrane reduces the effect of the magnetic pressure and decreases the membrane deflection. Some hysteresis of the membrane deflection under magnetic field could be observed, even at very low frequency (<1 Hz). The hysteresis observed with membrane deflection could be due to several factors: visco-elastic properties of the membrane material, of the tensile strength of the membrane (drum effect), of the viscosity of the liquid (in our case water + liquid soap). However, the DMA measurements (Fig. 8) show a small variation of the elastic modulus as a function of mechanical excitation frequency. This means that the visco-elastic properties of the membrane material should not be the most significant factor contributing to the hysteresis.

As a first approximation, considering that the shape of the deformed membrane looks like a spherical cap (this is true for large deflections) and knowing the inner diameter a_1 of the tube ($a_1 = 1.92$ mm) and the radius a of the membrane (a = 9 mm), it is easy to calculate from the liquid level h_1 in the tube (Fig. 10), the maximum deflection h_2 of the center of the membrane. h_2 is the real root of the following relationship:

$$h_2^3 + 3a_2^2 h_2 - (3a_1^2 h_1/2) = 0 \tag{1}$$

Figure 11 gives the magnetic field as the function of the deflection h_2 of the membrane. The maximum deflection obtained was about 0.682 mm for H = 1 Tesla. The difference in the response between the magnetic loading and the unloading is certainly due to the visco-elastic behavior of the material (the unloading rate is slow compared to the loading rate) and of the viscosity of the liquid in the tube. The general relationship between the magnetic pressure and the maximum deflection h_m of a circular isotropic membrane is given by:

$$\frac{\mu_0}{2} f \chi_p \mathrm{grad}(H^2) = \left(\frac{16}{3}\frac{E(f)}{1-\nu^2(f)}\frac{e^2}{a^4} + C_2\frac{\sigma_0}{a^2}\right)h_m + C_1(\nu)\frac{E(f)}{1-\nu(f)}\frac{h_m^3}{a^4} \tag{2}$$

In this relation a is the membrane radius, e the membrane thickness, E the Young modulus of the tested material, ν the Poisson ratio, σ_0 the mean residual stress in the membrane, f the content of magnetic particles, χ_p the magnetic susceptibility of the particles, μ_0 the magnetic

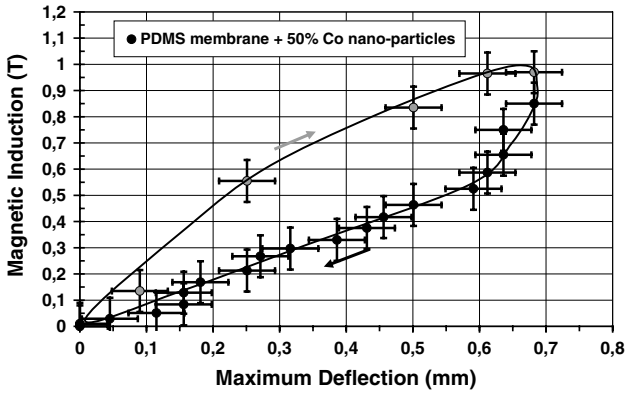

Fig. 11 Behavior of the membrane: applied magnetic field as a function of the maximum deflection of the membrane. The loading rate is about five times the unloading rate (0.4 T/s for the loading and 0.08 T/s for the unloading). The maximum value is about 0.68 mm for H = 1 T

permeability and grad (H^2) the gradient of the square of the magnetic field H. C_1 and C_2 are two constants which are respectively close to $C_1 \sim 2.88(1-\nu)$ and $C_2 \sim 4$. Two different cases have to be considered:

– Linear case when the deflections are small ($h_m < 0.3e$). The second term of the right member of the previous relation is negligible, thus:

$$h_m = \frac{\frac{\mu_0}{2} f \chi_p \, \mathrm{grad}(H^2)}{\left(\frac{16}{3}\frac{E(f)}{1-\nu^2(f)}\frac{e^2}{a^4} + C_2\frac{\sigma_0}{a^2}\right)} \quad (3)$$

h_m is proportional to grad (H^2) and inversely proportional to the mean stress value σ_0. Thus, from a technological point of view, to maximize h_m, σ_0 should be equal to zero or slightly negative, in any case smaller than the compressive buckling stress. When σ_0 is equal to zero, then:

$$h_m = \frac{3}{32}\frac{\mu_0 f \chi_p (1-\nu^2(f)) a^4}{E(f) e^2}\mathrm{grad}(H^2) \quad (4)$$

– Non linear case when the defections are high ($h_m \gg 0.3e$). The linear part of the general equation is negligible and if σ_0 is equal to zero, thus:

$$h_m = \left[\frac{\mu_0 f \chi_p}{2C_1(\nu)}\frac{(1-\nu(f))a^4}{E(f)}\mathrm{grad}(H^2)\right]^{1/3}.$$
$$\text{If } H(r) = H_0^n g(r) \text{ then:} \quad (5)$$
$$\frac{h_m^3}{fa^4} = \frac{\mu_0 \chi_p (1-\upsilon(f))}{2C_1(\upsilon)E(f)} H_0^{2n}\mathrm{grad}(g^2(r)).$$

h_m varies as $(\mathrm{grad}(H^2))^{1/3}$ and is proportional to $f^{1/3}$ and $a^{4/3}$. This domain is very different to the previous one due to the exponent 1/3 and generally applicable to the experimental data as $h_m/e \gg 1$.

To compare our results with those of the literature (Table 3) and where a, e, hm, f and H are accessible, according to the last equation the ratio $h_m^3 E/fa^4$ has been plotted as a function of the square of the magnetic field H_0^2. This representation is given in Fig. 12. Although χ_p (f) and g(r) are unknown a general trend is observed over 5 decades on the Y axis for a H_0 variation of about two decades. This tendency follows the relation: $Y = \alpha(H_0^2)^{1.5} = \alpha H_0^3$ (thus n = 1.5) which is to be compared to the last relation: $Y \approx H_0^{2n}\,\mathrm{grad}\,(g^2(r))$, with r being the distance of the considered point with respect to the origin. The translations

Table 3 Comparison of magnetic membranes for actuation in microfluidic devices

Magnetic membrane	Diameter 2a (mm)	Thickness e (μm)	Displacement h_m (μm)	External magnetic field	References
PDMS + small magnets (Ni80Fe20)	2	40	80	0.356 T	Bohm et al. 2001
PDMS + NdFeB/N48	10	500	–	–	Evans et al. 2007
PDMS + permalloy, Ni80Fe20	–	40	37.5	12.25 μN	Fahrni et al. 2009
PDMS + ferrite grains, carbonyl iron particles and magnetic NPs extracted from ferrofluids	–	110–160	180	450 Pa magnetic pressure	d'Agostino(1990)
PDMS + iron-oxide NPs	5	300	–	10 mT to 0.4 T	Oh and Ahn 2006
PDMS + iron-oxide NPs	4–7	35.5	135–625	0.416 T	Pirmoradi et al. 2010
PDMS with coil-shaped electrical path	3	11	51	0.09 T	Jackson et al. 2001
PDMS + Co NPs (16 % and 25 %)	50	250	400 (16 % Co) 800 (25 % Co)	0.04 T 0.04 T	Singh et al. 2013
Our results: PDMS + Co NPs (50 %)	18	400	~92* 612–682*	0.14 T 0.98 T	This study

NP nanoparticle

* Values calculated from the graph of Fig. 12 for the two extreme values of the magnetic field

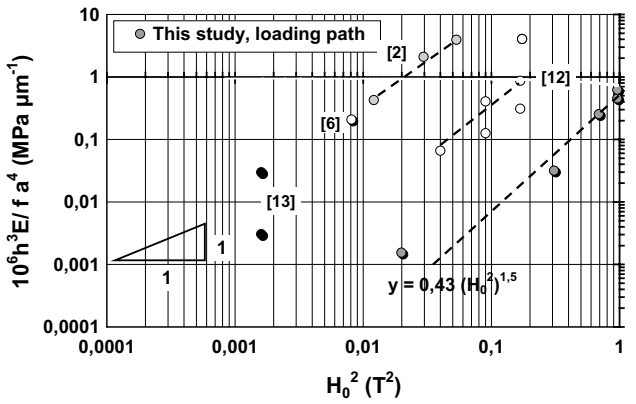

Fig. 12 Synthesis of the experimental data obtained on circular membranes with different dimensions. Concerning this study the five calculated points for the loading path (Fig. 11) are reported in this representation and follow the general tendency

between the different straight lines representative of the different works can be attributed to the values of the gradient (grad (g^2(r)) and of the value of the residual stress σ_0 inside the membrane (see the general Eq.(2)).

4 Conclusion and perspectives

The novel aspect of this work concerns the use of magnetically responsive elastomer material based on lab-synthesized magnetic Co nanoparticles as membrane for magnetically-actuated valve. Nanocomposite Co/PDMS membranes can be easily integrated in a PDMS device, using the same microfabrication technologies as for virgin PDMS, which allows manufacturing small valve with a large opening while reducing fabrication complexity and cost. The technology presented above can be advantageously applied to applications where simple and low-cost fabrication process for membrane-based fluidic actuator is required, such as disposable fluidic devices. Magnetic actuation is favorable as it generates large and long-range forces. It therefore allows for remote operation of the micro valve without any external or internal wire connection and makes the operation simple, as no precise alignment is required between the external magnet and the valve.

The main results of this work are summarized below:

1. Co-PDMS nano-composite magnetic membranes were fabricated with varying concentration of cobalt nanoparticles in PDMS matrix from 15-wt% to 75-wt% and characterized in term of mechanical and visco-elastic properties using DMA method. The best membrane was obtained with 50-wt% Co loaded in the PDMS matrix.
2. Loading of PDMS with cobalt nanoparticles allowed a wider range of control of the wetting properties of PDMS surfaces under oxygen plasma treatment, from hydrophobic to hydrophilic to super-hydrophilic. A contact angle down to 5° could be obtained for 50-wt% cobalt nanoparticles-embedded PDMS membrane treated for 30 min at high power (50 W).
3. A simple flow-through valve has been designed to demonstrate the feasibility of magnetic actuation with the 50-wt% Co PDMS membrane.
4. No deflection of the valve membrane was obtained in the area where the magnetic field inside the electromagnet is uniform.
5. In the region where the magnetic field gradient is the highest (up to 7.3 10^{-2} T/mm), high deflection of the composite membrane could be obtained (up to 0.68 mm for 1 Tesla). This result is very competitive with other work from the literature. However some hysteresis of the membrane defection could be observed, even at very low frequency.
6. It is of course important to reduce this hysteresis, which is energy not used in the actuation of the device. Taking into account that fluid composition is often imposed by the experiment and cannot be changed at will, possible ways to reduce the hysteresis include increasing the tensile strength of the membrane. In this case, a compromise must be found for efficient magnetic actuation and low hysteresis value.
7. Another origin of this hysteresis can be a phase difference between the applied magnetic field and its gradient. This hypothesis must be supplemented by other experiments and/or by a more accurate modeling of the magnetic effort that act on this membrane. This latter can be useful in order to understand and optimize the magnetic field action and its gradient on magnetic membrane.

Acknowledgments The authors would like to thank M. Shirolkar and Prof. S. K. Kulkarni, from Pune University, for the synthesis of the cobalt nanoparticles.

This work was carried out within the framework of the Programme IFCPAR (# 3408-01) and the Programme Inter Carnot-Fraunhofer "3 µP: Multi-Reaction, Multi-Sample Microfluidic Platform".

A. Singh would like to thank 3 µP for the financial support.

References

Berthier J, Ricoul F (2004) Development of micromembranes as actuators in Microsystems. Appl Nanosci 1:31–38

Bohm S, Olthuis W, Bergveld P (2001) A plastic micropump constructed with conventional techniques and materials. Sens Actuators A 77:223–228

d'Agostino R (1990) Plasma deposition, treatment, and etching of polymers. Academic Press Inc., San Diego

Evans BA, Shields AR, Lloyd Carroll R, Washburn S, Falvo MR (2007) Superfine, magnetically actuated nanorod arrays as biomimetic cilia. Nano Lett 7:1428–1434

Fahrni F, Prins MWJ, Van IJzendoorn LJ (2009) Magnetization and actuation of polymeric microstructures with magnetic nanoparticles for application in microfluidics. J Magn Magn Mater 321:1843–1850

Gaspar A, Piyasena ME, Daroczi L, Gomez FA (2008) Magnetically controlled valve for flow manipulation in polymer microfluidic devices. Microfluid Nanofluid 4:525–531

Jackson WC, Tran HD, O'Brien MJ, Rabinovich E, Lopez GP (2001) Rapid prototyping of active microfluidic components based on magnetically modified elastomeric materials. J Vac Sci Technol B 19:596–599

Khoo M, Liu C (2001) Micro magnetic silicone elastomer membrane actuator. Sens Actuators A 89:259–266

Lee W, Lee SS (2007) Focal tunable liquid lens integrated with an electromagnetic actuator. Appl Phys Lett 90:121129–121131

Oh KW, Ahn CH (2006) A review of microvalves. J Micromech Microeng 16:R13–R39

Pirmoradi F, Cheng L, Chiao M (2010) A magnetic poly(dimethylesiloxane) composite membrane incorporated with uniformly dispersed, coated iron oxide nanoparticles. J Micromech Microeng 20:015032–015037

Singh A, Shirolkar M, Limaye MV, Gokhale S, Khan-Malek C, Kulkarni SK (2013) A magnetic nano-composite soft polymeric membrane. Microsys Technol 19:409–418

Yamahata C, Lacharme F, Gijis MAM (2005) Glass valveless micropump using electromagnetic actuation. Microelectro Eng 78–79:132–137

Yang HT, Su YK, Shen CM, Yang TZ, Gao HJ (2004) Synthesis and magnetic properties of e-cobalt nanoparticles. Surf Interface Anal 36:155–160

Yin HL, Heng YC, Fang W, Hsieh J (2007) A novel electromagnetic elastomer membrane actuator with semi embedded coil. Sens Actuators A 139:194–202

Yu JH, Lee DW, Kim BK, Jang T (2006) Synthesis and properties of magnetic fluid based on iron nanoparticles prepared by a vapor-phase condensation process. J Mag Mag Mat 304:16–18

Yufeng S, Wenyuan C, Feng C, Wieping Z (2006) Electro-magnetically actuated valveless micropump with two flexible diaphragms. Int J Adv Manu Technol 30:215–220